Bioactive Materials 47 (2025) 502–512

Contents lists available at ScienceDirect

Bioactive Materials

journal homepage: www.keaipublishing.com/en/journals/bioactive-materials

A self-sacrificing anti-inflammatory coating promotes simultaneous cardiovascular repair and reendothelialization of implanted devices

Pai Peng [a], Shili Ding [b], Min Liang [c], Weiwei Zheng [a], Yongyuan Kang [a], Wenxing Liu [a], Haifei Shi [b,**], Changyou Gao [a,c,d,*]

[a] MOE Key Laboratory of Macromolecular Synthesis and Functionalization, Department of Polymer Science and Engineering, Zhejiang University, Hangzhou, 310058, China
[b] Department of Hand Surgery, First Affiliated Hospital of Zhejiang University, School of Medicine, Hangzhou, 310003, China
[c] Center for Healthcare Materials, Shaoxing Institute, Zhejiang University, Shaoxing, 312099, China
[d] The State Key Laboratory of Transvascular Implantation Devices, Zhejiang University, Hangzhou, 310009, China

ARTICLE INFO

Keywords:
Immuno-modulating biomaterials
Self-sacrificing coating
Anti-inflammation
Pro-endothelialization
Cardiovascular implant

ABSTRACT

During interventional surgeries of implantable cardiovascular devices in addressing cardiovascular diseases (CVD), the inevitable tissue damage will trigger host inflammation and vascular lumen injury, leading to delayed re-endothelization and intimal hyperplasia. Endowing cardiovascular implants with anti-inflammatory and endothelialization functions is conducive to the target site, offering significant tissue repair and regeneration benefits. Herein, inspired by the snake's molting process, a ShedWise device was developed by using the poly (propylene fumarate) polyurethane (PPFU) as the foundational material, which was clicked with hyperbranched polylysine (HBPL) and followed by conjugation with pro-endothelial functional Arg-Glu-Asp-Val peptide (REDV), and finally coated with a "self-sacrificing" layer having reactive oxygen species (ROS)-scavenging ability and degradability. During the acute inflammation in the initial stage of implantation, the ROS-responsive hyperbranched poly(acrylate-capped thioketone-containing ethylene glycol (HBPAK) coating effectively modulated the level of environmental inflammation and resisted initial protein adsorption, showcasing robust tissue protection. As the coating gradually "sacrificed", the exposed hyperbranched HBPL-REDV layer recruited specifically endothelial cells and promoted surface endothelialization. In a rat vascular injury model, the ShedWise demonstrated remarkable efficiency in reducing vascular restenosis, protecting the injured tissue, and fostering re-endothelization of the target site. This innovative design will introduce a novel strategy for surface engineering of cardiovascular implants and other medical devices.

1. Introduction

Cardiovascular disease (CVD) has become the leading cause of death worldwide [1–3]. To address cardiovascular diseases and their associated organ and tissue pathologies, various types of implantable cardiovascular devices such as artificial heart valves, vascular stents, ventricular assist devices, and catheters are widely utilized [4–8]. However, all interventional surgical procedures would inevitably cause vascular injury characterized by denudation of the endothelial cell layer, which typically serves as an effective barrier against thrombosis, lipid uptake, and inflammatory cell infiltration [9,10]. Nonetheless, some typical interventional therapies remain the gold standard for treatment. For example, drug-eluting stents (DES) have been implanted in millions of patients, effectively reducing the incidence of early in-stent restenosis (ISR) due to the loading of anti-proliferative drugs [11–13]. However, the released drugs inhibit endothelial cell growth, exacerbating the endothelial injuries caused by interventional surgeries, which subsequently leads to difficulties in achieving eventual endothelialization. The lack of a natural endothelial barrier increases the risk of long-term thrombosis, predisposing to late-stage intimal hyperplasia [14–16].

Peer review under the responsibility of KeAi Communications Co., Ltd.
* Corresponding author. MOE Key Laboratory of Macromolecular Synthesis and Functionalization, Department of Polymer Science and Engineering, Zhejiang University, Hangzhou, 310058, China.
** Corresponding author. Department of Hand Surgery, First Affiliated Hospital of Zhejiang University, School of Medicine, Hangzhou, 310003, China.
E-mail addresses: shihaifei@zju.edu.cn (H. Shi), cygao@zju.edu.cn (C. Gao).

https://doi.org/10.1016/j.bioactmat.2025.01.037
Received 25 November 2024; Received in revised form 27 January 2025; Accepted 27 January 2025

In the case of vascular stent implantation, the initial disturbance of blood flow leads to complex spatiotemporal changes in shear stress, resulting in increased thrombogenicity and alterations in endothelial phenotype from quiescent to inflammatory. This promotes inflammatory cell migration and escalates oxidative stress significantly, leading to tissue and cellular damage [17–19]. The acute inflammatory response interacts with the coagulation response, exacerbating each other [20]. Due to the unmitigated adverse microenvironment resulting from early lipid uptake and inflammatory cell migration, the disturbed vascular cell behaviors foster late-stage stent thrombosis and the progression of atherosclerosis [21,22].

Given the close association between inflammation and excessive production of reactive oxygen species (ROS) at the intervention site, the use of antioxidants to eliminate ROS emerges as a promising approach to regulate the vascular pathological microenvironment [23,24]. However, excessive antioxidant therapy may deplete the appropriate levels of inflammation and ROS, unfavorably affecting normal endothelial repair and vascular remodeling. Encouragingly, an increasing number of researchers suggest that ROS-responsive strategies can mitigate excessive pathological ROS production while preserving physiological ROS levels, achieving an adaptive regulation of the inflammatory environment [25–28].

Inspired by the snake's remarkable molting process, ShedWise is endowed with a self-adaptive, self-sacrificing coating designed to provide early-stage protection and foster regeneration in the later stage. The name "ShedWise" reflects the intelligent design of the coating, drawing a direct parallel to the snake's natural ability to shed its outer layer as a defense and renewal mechanism. Its efficacy in protection in the earlier stage and promotion of endothelialization in the late stage is demonstrated *in vitro* and *in vivo*. The ShedWise utilizes an unsaturated and degradable polyurethane (PPFU) as a substrate, which is synthesized from poly(propylene fumarate) (PPF) diol and hexane diisocyanate (HDI) with the ease of modification, biodegradability and desired mechanical properties [29]. A pro-endothelial functional layer is constructed by covalent grafting of hyperbranched polylysine (HBPL) via Michael addition, followed by conjugation with pro-endothelial functional Arg-Glu-Asp-Val peptide (REDV). A ROS-responsive poly(acrylate-capped thioketone-containing ethylene glycol (HBPAK) containing multiple thioketal (TK) linkages is then used to create the top "self-sacrificing" hydrogel coating. The "self-sacrificing" layer scavenges ROS primarily through the TK linkages in HBPAK. These TK linkages are highly sensitive to various types of ROS such as O_2^- and H_2O_2, even at low concentrations (e.g., 100 μM H_2O_2), whereas stay stable to acid-, base- and protease-catalyzed degradation, ensuring stability in other physiological processes [30–33]. Upon exposure to ROS, the TK bonds undergo redox reactions, generating sulfhydryl and acetone as the byproducts. This reaction not only scavenges ROS but also causes the degradation of the HBPAK-based "self-sacrificing" layer. During the acute inflammation phase in the early implantation stage, the outermost gel coating resists initial protein adsorption and regulates environmental inflammatory level through its hydrophilicity, and ROS-scavenging and degradation nature, thereby protecting tissues and establishing the groundwork for subsequent endothelialization. As the coating gradually "sacrifices", the specific pro-endothelial layer of HBPL-REDV comes into play, promoting the formation of a natural endothelial barrier. Hence, the cascade process of "protecting-sacrificing-pro-endothelialization" is accomplished by our ShedWise (Scheme 1). The performance of ShedWise is demonstrated *in vitro* and *in vivo*. The current design not only provides a novel strategy for surface engineering of cardiovascular devices, but also is applicable to other devices necessitating anti-inflammation and tissue regeneration.

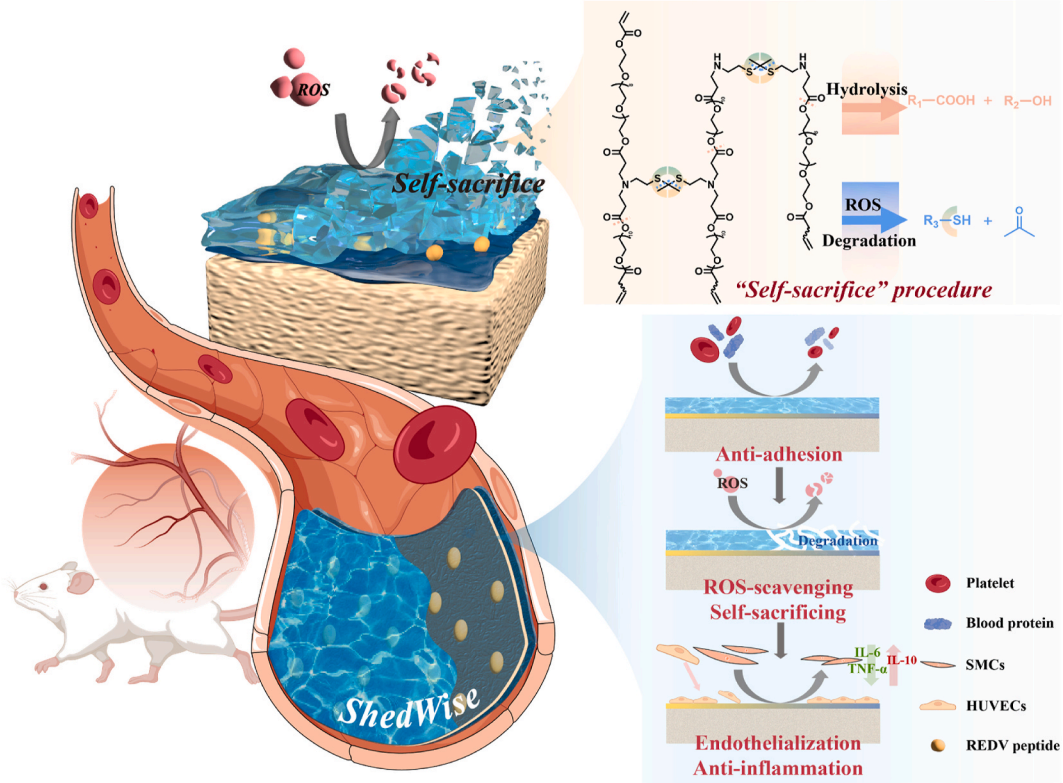

Scheme 1. Schematic illustration of vascular injury repaired by the "multi-in-one" device of ShedWise. A hyperbranched poly(acrylate-capped thioketone-containing ethylene glycol (HBPAK) is introduced to modulate environmental inflammation and resist initial protein adsorption. As the coating gradually "sacrifices" due to the reaction with environmental ROS, the exposed hyperbranched poly-lysine/Arg-Glu-Asp-Val peptide (HBPL-REDV) layer promotes surface endothelialization, forming a natural endothelial barrier. This composite cardiovascular implant coating efficiently takes an anti-inflammatory role and facilitates the re-endothelialization process of the injured vascular tissue.

2. Results and discussion

2.1. Construction and characterization of ShedWise

The ShedWise was constructed following the steps shown in Fig. 1a by using HBPL, Cys-Arg-Glu-Asp-Val peptide (REDV-SH), methacrylated hyaluronic acid (HAMA), and HBPAK (Figures S1-3). Along with the increase in HBPL concentration, the grafting density of HBPL on PPFU increased to 6.1×10^{-8} mol/cm^2 until 75 mg/mL, and then decreased at a still higher concentration (Fig. S4a). The water contact angle (WCA) of PPFU declined from 88.3 ± 5.0° to 63.7 ± 2.5° after HBPL grafting regardless of its concentration (Fig. S4b), revealing the more hydrophilic nature of PF-HB. The WCA is governed mainly by the very superficial layer of substrate, which explains the independence of the grafting amount of HBPL. Therefore, 75 mg/mL of HBPL was chosen in the next study.

The successful HBPL grafting was also confirmed by X-ray photoelectron spectroscopy (XPS) (Fig. 1b and c) and attenuated total reflection Fourier-transform infrared (ATR-FTIR) spectroscopy (Fig. S4c) according to the appearance of -NH_2 peak at 401 eV, and enhanced C-H stretching vibration at 2972 cm^{-1} and carbonyl peak at 1721 cm^{-1}. By using a silicon wafer as the substrate, the thickness of the grafted HBPL layer was examined to be 5.8 nm by ellipsometry (Fig. 1d).

Next, the PF-HB surface was grafted with sulfhydryl-containing REDV-SH peptide via the -SH and -NH_2 condensation reaction under succinimidyl 4-[N-maleimidomethyl] cyclohexane-1 carboxylate (SMCC) catalyzation to obtain the PF-H/R. The grafting amount of REDV-SH was measured as 233.4 ng/cm^2 by a quartz crystal microbalance with dissipation (QCM-D) (Fig. 1e).

On the PF-H/R substrate, the self-sacrificing coating was constructed through a classical interface interpenetrating strategy [34,35]. The hydrophilic HBPL functions as a mediator to help the pre-gel solution spread and diffuse into the substrate, forming a robust hydrogel coating eventually. Here, the bonding mechanism relied on the interpenetration of the gel network into the functionalized substrate. The hydrophilicity imparted by HBPL and REDV-SH modification facilitated the swelling of the polymer substrate. Benzophenone (BP) enhanced this effect, loosening the interface layer and allowing partial gel network infiltration. This formed a robust double-mesh anchoring structure, ensuring strong adhesion between the hydrogel and substrate. Along with the increase in

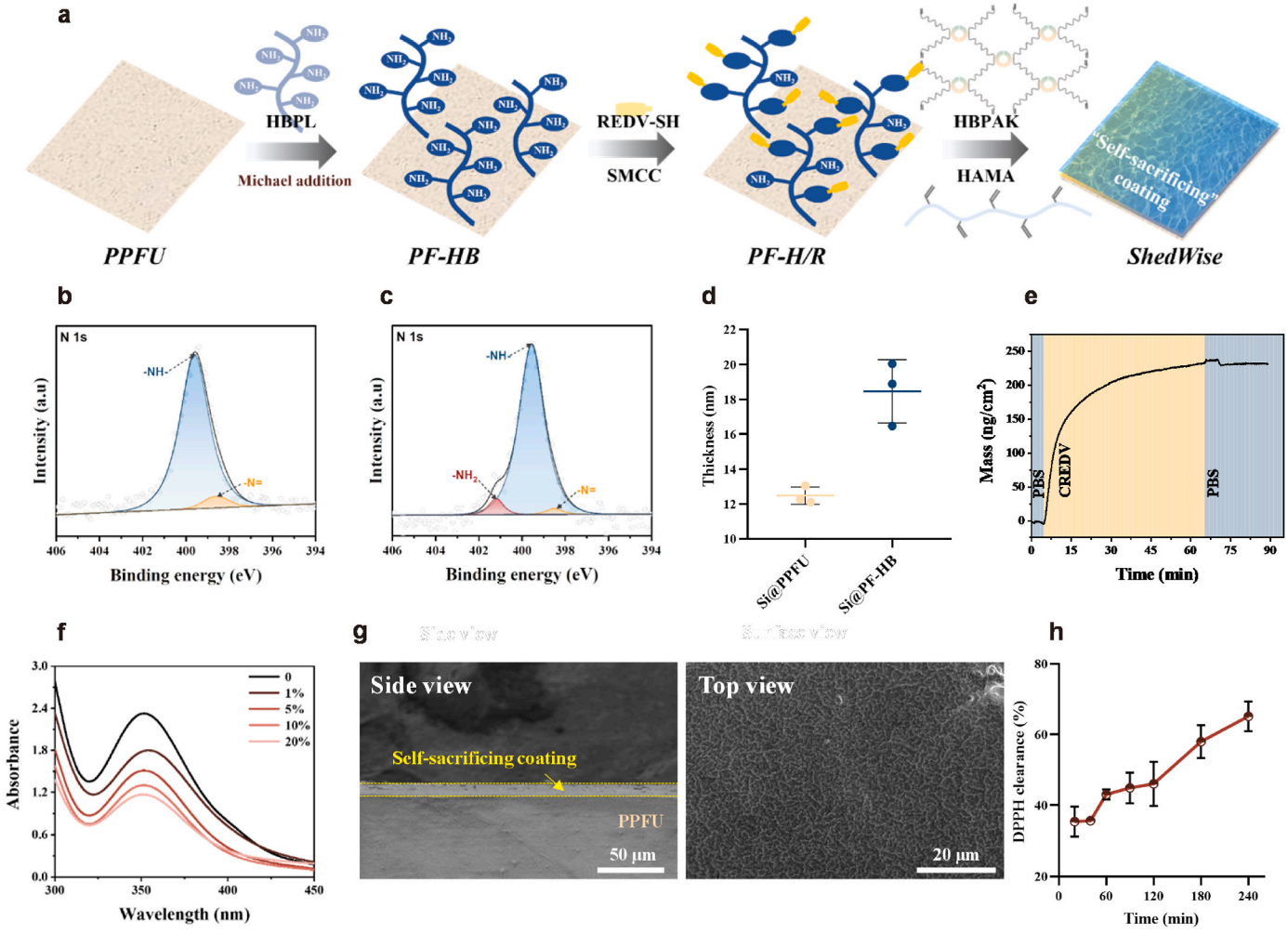

Fig. 1. Construction and characterization of ShedWise. (a) Schematic illustration of the preparation process of ShedWise. The poly(propylene fumarate) polyurethane (PPFU) with unsaturated carbon double bonds in its main chain is clicked with HBPL via Michael addition to obtain PF-HB, followed by covalent binding of Cys-Arg-Glu-Asp-Val peptide (REDV-SH) via -NH_2 and -SH condensation under the catalyzation of succinimidyl 4-[N-maleimidomethyl] cyclohexane-1 carboxylate (SMCC) to obtain PF-H/R. HBPAK and methacrylated hyaluronic acid (HAMA) solution is then coated onto the PF-H/R surface, followed by UV-irradiation to obtain the final ShedWise product. N 1s core-level XPS spectra of PPFU membrane before (b) and after (c) HBPL grafting. (d) Changes in sample thickness before and after HBPL grafting measured by ellipsometer (Si@PPFU refers to silicon wafer spin-coated by PPFU on the surface) (n = 3). (e) QCM-D curve showing the grafting mass of REDV-SH peptide along with time prolongation. (f) UV absorption of H_2O_2/KI solutions being treated by coatings with different HBPAK concentrations at 0, 1 %, 5 %, 10 % and 20 % (m/v). (g) Representative image of the side view and top view of ShedWise by SEM. (h) Clearance of DPPH (200 μM) by ShedWise (d = 10 mm) along with time prolongation (n = 3).

HBPAK concentration, the elimination rate of 10 μM H_2O_2 also increased gradually (Fig. 1f).

Through preliminary optimization experiments, we found that 5 % (m/v) of HBPAK provided a consistent and stable coating, with sufficient antioxidative capacity to modulate the inflammatory environment while maintaining the reproducibility of the preparation process. Therefore, 5 % (m/v) of HBPAK was chosen to prepare the ShedWise. The thickness of the hydrogel layer was estimated as 10.2 μm by the cross-section scanning electron microscopy (SEM) image (Fig. 1g), where the crack-like pattern on the top view image attests to the formation of a self-sacrificing coating, akin to the hydrogel coatings demonstrated in previous studies [36,37]. Moreover, the ShedWise constructed from fluorescein isothiocyanate (FITC)-labeled HBPAK showed the fluorescence emission peaking at 530 nm (Fig. S5a), substantiating the existence of hydrogel coating. The measured thickness of 7.9 ± 3.8 μm (Fig. S5b) is comparable to the coatings found on drug-eluting stents (DES) in commercial applications [38].

Furthermore, the surface atom analysis for every step of the construction was determined by XPS (Table 1). The PF-RE served as a control group, where REDV-SH was directly fixed to the PPFU surface through a click reaction. The changes in surface elemental compositions are well aligned with the reaction mechanisms. Specifically, the significant increase in N content (6.59 at%) and the higher N/C ratio (9.35 %) in PF-HB reflect the introduction of HBPL, which is rich in amino groups. After conjugation with the REDV-SH peptide, the N content (6.26 at%) and N/C ratio (8.91 %) remain high, indicating the retention of hyperbranched structures. The notable increase in sulfur content (0.95 at%) and S/C ratio (1.35 %) confirms the effective incorporation of the sulfur-contained REDV-SH peptide. Following the application of the "self-sacrificing" coating, the N content decreases to 2.35 at%, while the S content remains at 0.91 at%, suggesting the stable presence of ROS-scavenging HBPAK moieties containing sulfur.

The adhesion of the self-sacrificing coating was determined using a 90-degree peel test, yielding an adhesion energy of 13.4 J/m^2 (Fig. S5c). This result aligns with the expected properties of hydrogel coatings that achieve substrate bonding through an interface interpenetrating strategy [37,39]. The anti-oxidation property of ShedWise was demonstrated by a 1,1-diphenyl-2-picryhydrazyl (DPPH) assay (Fig. 1h). Along with time prolongation, the purple color of the DPPH solution gradually faded. After 240 min, 65.1 ± 3.7 % DPPH was scavenged by a 10 mm diameter sample of ShedWise. In contrast, the PF-H/R group maintained a distinct residual color under the same reaction condition (Fig. S5d).

2.2. Degradation behaviors of the self-sacrificing coating

As demonstrated by previous studies on intravascular stent coatings, achieving a controlled degradation profile is essential for maintaining vascular functionality during repair [40–42]. The ShedWise coating aligns with this principle by employing a self-sacrificing layer, which can eliminate ROS and is simultaneously decomposed under oxidative stress as demonstrated by static and dynamic simulative experiments *in vitro*. The decomposition of one thioketal linkage in HBPAK results in a bimolecular sulfhydryl compound and one acetone. Fig. S5e shows that under static oxidative conditions, the acetone concentration increased over time, indicating gradual coating degradation, the curves reached a platform at 36 h and 48 h for the coating with 5 % and 10 % HBPAK, respectively. As expected, a higher concentration of HBPAK also generated a larger amount of acetone.

Table 1
Surface atom analysis of different groups measured by XPS.

Groups	Surface composition (at%)				Element ratio	
	C	N	O	S	N/C × 100%	S/C × 100%
PPFU	64.79	2.03	33.18	/	3.13	/
PF-HB	70.45	6.59	22.96	/	9.35	/
PF-RE	66.74	4.42	28.72	0.12	6.62	0.18
PF-H/R	70.24	6.26	22.55	0.95	8.91	1.35
ShedWise	65.13	2.35	31.60	0.91	3.61	1.40

Under the simulated oxidative circulation condition, the dynamic degradation process was demonstrated (Fig. 2). Cracks appeared on the hydrogel coating at 12 h, which developed into multiple and larger ones, resulting in the ultimate disintegration of the whole coating (Fig. 2a). Quantitative analysis in Fig. 2b revealed that the ShedWise had a higher slope of degradation at first 120 h, which was slowed down until equilibrium was reached at 200 h. By contrast, the degradation rate of non-responsive PEGDA/HAMA coating remained below 20 %, which should be mainly caused by the hydrolysis of the acrylate structure. In summary, under simulated oxidative stress the self-sacrificing coating was completely degraded at 8 d, which aligns with the ROS dynamics observed in vascular injury models, where ROS peaks on day 1 and then decreases by day 3 and day 7 [43]. This design ensures sufficient antioxidant protection during the ROS-active period and timely degradation. Previous studies also demonstrate that HAMA hydrogels without HBPAK show minimal degradation in 250 mM H_2O_2, while introducing HBPAK leads to significant mass loss (over 60 % in 10 days). This highlights the role of HBPAK in promoting degradation under oxidative conditions. Additionally, hydrogels with HBPAK degrade much slower in PBS compared to H_2O_2, indicating that ROS significantly influence its degradation rate [44]. These findings support the tunability of coating degradation via HBPAK ratio and ROS levels. Therefore, the premature depletion of the top hydrogel coating and early exposure of the pro-endothelial layer under high inflammation can be mitigated by adjusting the HBPAK concentration to prolong the degradation process. This adjustment provides effective protection against excessive ROS and delays the functional layer exposure during the inflammatory peak, ensuring the top coating maintains its anti-inflammatory properties while allowing controlled exposure of the pro-endothelial layer.

To address the varying activities of different ROS, we conducted additional experiments using activated neutrophils to simulate the ROS-rich environment following vascular injury [45]. Neutrophils isolated from the peripheral blood of C57 mice were stimulated with phorbol 12-myristate 13-acetate (PMA) to produce reactive oxygen species (ROS) via nicotinamide adenine dinucleotide phosphate (NADPH) oxidase, mimicking the early inflammatory response. As shown in Fig. S6, noticeable pores and fractures appeared in the coating after 24 h, indicating ROS-responsive degradation. By 48 h, interconnected pores and extensive degradation were observed, demonstrating the adaptive degradability of our sacrificial coating in response to diverse ROS environments.

To verify the retention of pro-endothelial layer structure after degradation of the self-sacrificing coating, the ATR spectra of ShedWise, PF-H/R, and ShedWise post-degradation were compared (Fig. S7a). The ester carbonyl peak of HBPAK at 1734 cm^{-1} shifted to a lower wavenumber (1720 cm^{-1}) after degradation, indicating the changes in the carbonyl environment, while the peak at 1100 cm^{-1} corresponding to C-O-C stretching vibration disappeared. A new peak at 1647 cm^{-1} (-CO-NH-) was detected in both PF-H/R and ShedWise post-degradation group, suggesting a similar surface structure. SEM characterization showed increased nitrogen content post-degradation (Fig. S7b), which was consistent with the XPS results, demonstrating the retention of the pro-endothelial functional layer after degradation of the sacrificing layer.

2.3. Hemocompatibility of ShedWise

Implantable cardiovascular devices always contact the complicated blood environment directly, where their surface takes the major role concerning hemocompatibility. The modification strategy here aims not only to minimize blood component destruction and potential impact on the coagulation process, but also to enhance the crucial anti-adhesion activity. A comprehensive evaluation of ShedWise was thus

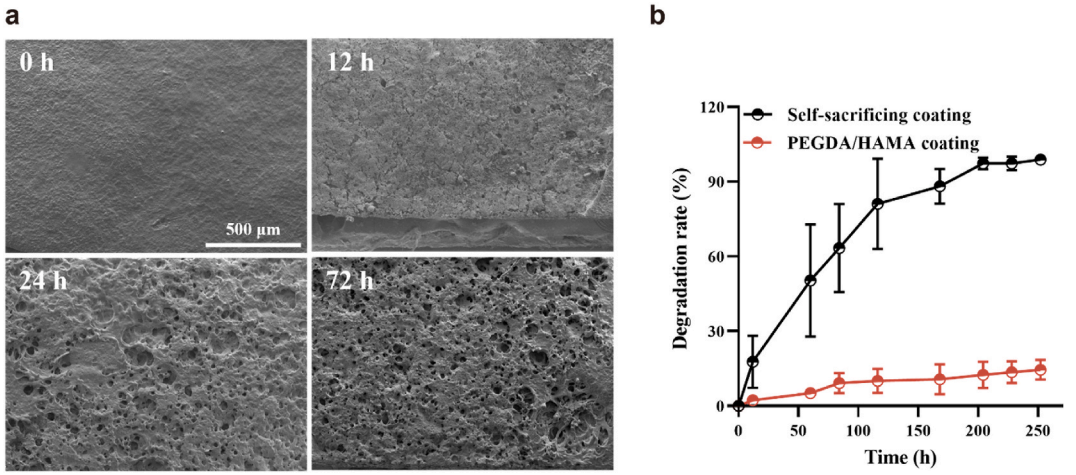

Fig. 2. Degradation behavior of the self-sacrificing coating. (a) Representative surface SEM images of ShedWise at different degradation time (0, 12, 24 and 72 h). (b) The degradation rate of self-sacrificing coating (5 % of HBPAK with 1 % of HAMA, m/v) and PEGDA/HAMA coating along with time prolongation (n = 3).

implemented in terms of erythrocyte-related hemocompatibility, blood clotting, and anti-platelet adhesion.

The extent of erythrocyte damage caused by blood-contacting biomaterials can be inferred from a higher hemolysis ratio. Here, the hemolysis ratios remained at critically low values of 0.16 ± 0.15 % (PPFU), 0.72 ± 0.20 % (PF-H/R), and 0.25 ± 0.14 % (ShedWise) as shown in Fig. 3a. The slightly higher ratio of the PF-H/R group is likely attributed to the interaction between the positively charged HBPL molecules and the negatively charged phospholipids on the erythrocyte membrane. Nonetheless, the hemolysis ratios are all far below the accepted threshold of 5 % for blood-contacting materials.

To investigate the effect of the modified coatings on the surrounding

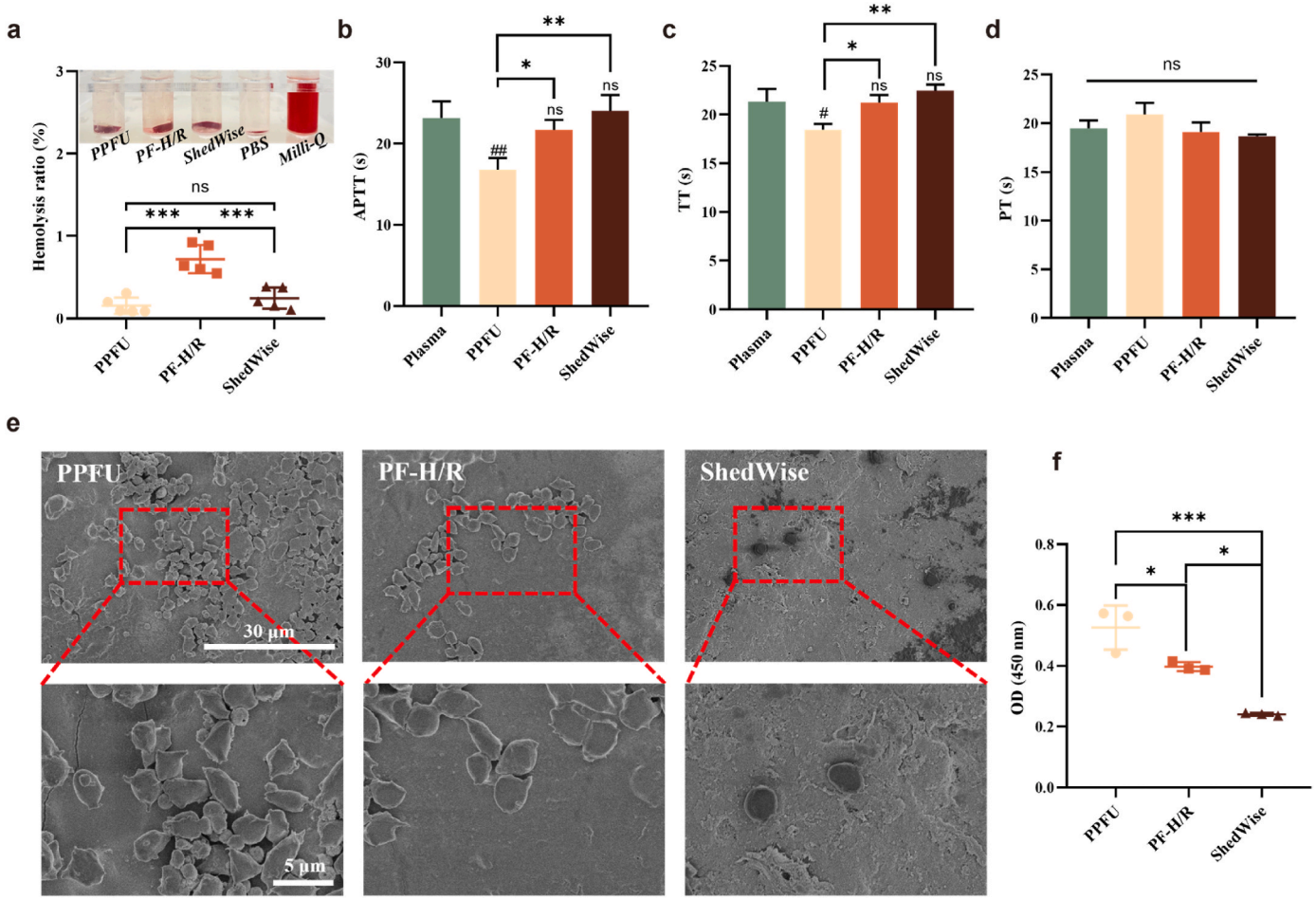

Fig. 3. Hemocompatibility of ShedWise. (a) Red blood cell hemolysis ratio of different groups (n = 5). Clotting time for different groups in (b) APTT, (c) TT, and (d) PT tests (n = 3). (e) Representative SEM images of samples after platelet adhesion. (f) Quantitative platelet adhesion results by LDH assay (n = 3). #p < 0.05 and ##p < 0.01 versus the Plasma group; *p < 0.05, **p < 0.01 and ***p < 0.001; ns = no significant difference.

blood coagulation cascade, activated partial thromboplastin time (APTT), prothrombin time (PT), and thrombin time (TT) were tested (Fig. 3b–d), respectively. Compared to those of PPFU, the APTT and TT of PF-H/R and ShedWise groups were significantly prolonged, whereas there was no significant difference in PT among all groups. These results showcase that the intrinsic and final common pathways in the coagulation cascade are prohibited, while the extrinsic pathway is not affected strongly. A more significant prolongation of ShedWise can be attributed to the restricted adhesion of necessary clotting factors for thrombin generation and fibrin clot formation onto the HBPAK-containing top coating, which is rich in PEG segments. The PEG-based coating minimizes protein adhesion and passively reduces the availability of clotting factors, thereby interfering with the enzymatic cascade required for coagulation [46]. It is worth mentioning that, compared to the original PPFU, the ultimate indices of the PF-H/R and ShedWise were almost the same as those of the plasma group, suggesting that the coagulation process will not be influenced after the coating formation.

The anti-adhesion property was assessed by exposing samples to platelet-rich plasma (PRP). The quantity and activation level of adhered platelets on the sample surfaces were examined using SEM (Fig. 3e) and lactate dehydrogenase (LDH) assay (Fig. 3f). The PPFU surface was covered by numerous irregularly shaped platelets with pseudopods extending. Conversely, the PF-H/R displayed a marginal decrease in adhered platelets count, attributable to the integration of hydrophilic HBPL. To some extent, this property imparts resistance against unspecific protein adsorption by selectively binding to plasminogen present in the plasma, thereby facilitating thrombus dissolution [47,48]. By sharp contrast, the adhesion of platelets was substantially decreased on ShedWise. Their morphology remained in the disk shape as more clearly shown in the higher magnification image, suggesting that the platelets were inactive due to the hydrophilic nature of the HBPAK-based coating. Consistent with this observation, a significantly higher optical density (OD) value was observed on PPFU (0.53 ± 0.06) and PF-H/R (0.40 ± 0.02) compared to ShedWise (0.24 ± 0.00) (Fig. 3f), demonstrating again that ShedWise can significantly reduce the platelet adhesion.

2.4. Cell protection capacity and anti-inflammatory efficacies in vitro

Cell survival is the prerequisite for a series of subsequent physiological activities. However, the excessive ROS environment could bring

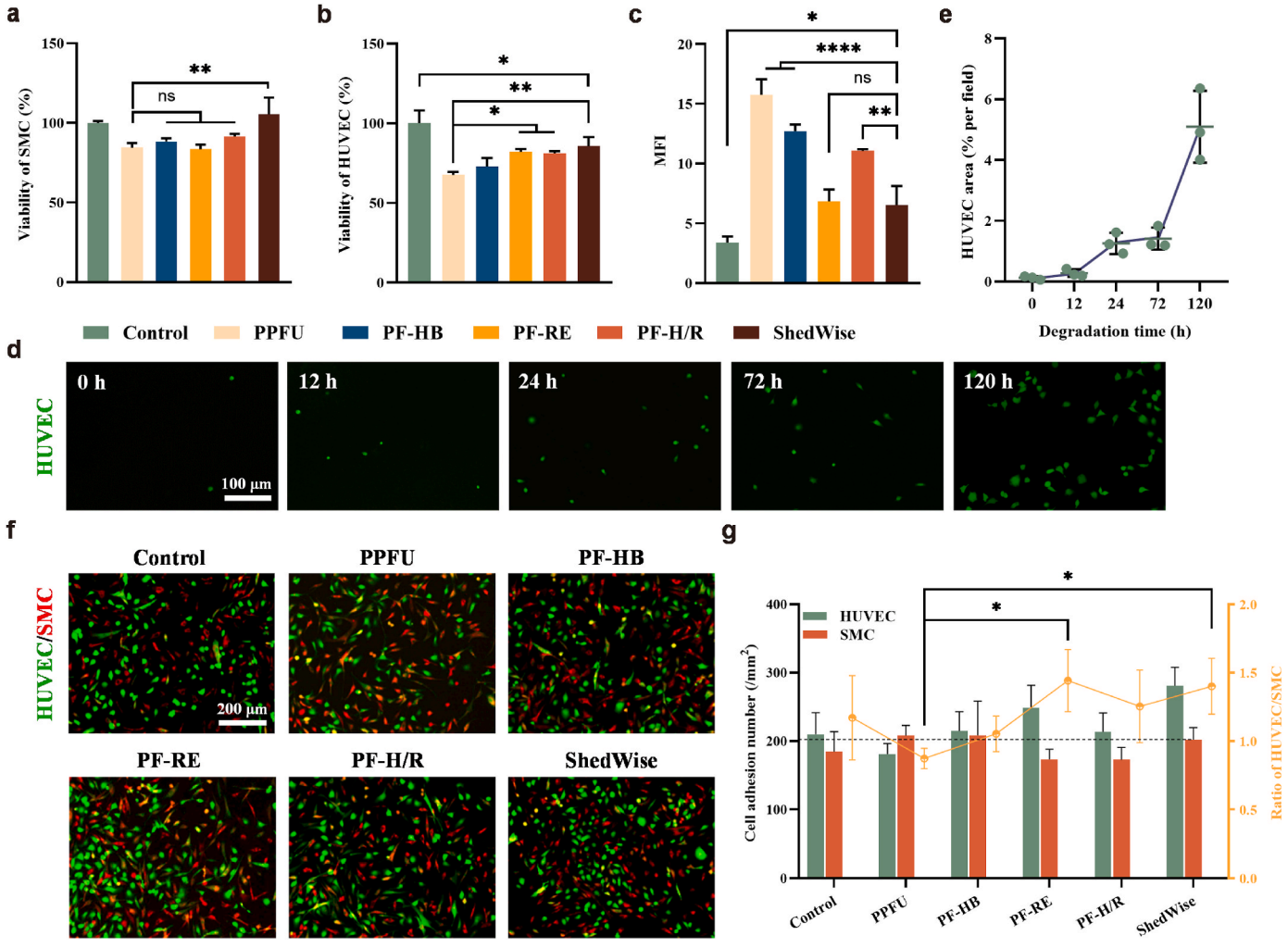

Fig. 4. Cell behaviors with different coatings *in vitro*. Viability of (a) SMC and (b) HUVEC on the sample surfaces under an oxidative environment (n = 3). The oxidative environment was established by adding H_2O_2 to the medium which had been co-cultured with cells for 24 h, achieving a final concentration of 0.2 mM, and lasting for 3 h "Control" refers to cells seeded on PPFU films without H_2O_2 treatment. (c) Mean fluorescence intensity (MFI) of HUVEC on different samples quantified from images in Fig. S12, showing the relative oxidative stress levels (n = 3). (d) Representative images of HUVEC adhesion on the ShedWise being treated with 0.2 mM H_2O_2 for 0, 12, 24,72, and 120 h, respectively. (e) HUVEC area on the ShedWise along with prolongation of H_2O_2-treatment time (n = 3). (f) Fluorescence images of co-cultured HUVEC (green) and SMC (red) being incubated on different samples. Cells were treated with 0.1 mM H_2O_2 for 12 h before co-culturing on the sterilized samples in a 24-well plate for 48 h. (g) Quantification of the cell adhesion (left Y axis) and the ratio of HUVEC/SMC (right Y axis) from images in (f), (n = 4). *p < 0.05, **p < 0.01 and ****p < 0.0001; ns = no significant difference.

serious inflammation damage and lead to apoptosis [49,50]. To assess the cytocompatibility, the proliferation of human umbilical vein endothelial cells (HUVEC) and smooth muscle cells (SMC) on the sample surfaces was pretested under a normal environment (Fig. S8), showcasing the normal cell adhesion and proliferation on all the sample surfaces without apparent cytotoxicity.

Cell counting kit-8 (CCK-8) assay revealed that ShedWise significantly enhanced the viability of SMC (Fig. 4a) and HUVEC (Fig. 4b) in an oxidative environment. The PF-RE and PF-H/R also significantly improved the viability of HUVEC. The REDV peptide is known to promote the adhesion of endothelial cells onto the matrix or among the cells, augmenting that the connection plays a pivotal role in sustaining a portion of cellular structure and functionality amidst oxidative surroundings, and thereby fortifying the resistance against oxidative injury [51]. By contrast, the PF-HB group did not exhibit an enhanced effect on the viability of endothelial cells in an oxidative environment. Therefore, the self-sacrificing coating can meliorate the oxidative environment, providing a protective effect on the proliferation of endothelial cells. This conclusion was further supported by the live (Calcein-AM, green)/dead (PI, red) assay (Fig. S9), where the extensive cell damage caused by H_2O_2 oxidation in the PPFU group was significantly remitted in the ShedWise group.

Next, the corresponding ROS inside HUVEC being cultured on different substrates were quantified (Fig. 4c and Fig. S10), showing consistent results of cell viability. Under the existence of H_2O_2, the PPFU group had a relatively weak ability to down-regulate the intracellular ROS level, whereas both the PF-HB and PF-H/R could to some extent. By contrast, the PF-RE and ShedWise could very significantly reduce the intracellular ROS levels. The REDV-SH grafting plays a role in improving endothelial cell function. The REDV peptide can specifically bind to α4β1 integrin on the surface of endothelial cell membrane, so that cells can play an antioxidant role by secreting antioxidant enzymes such as superoxide dismutase and catalase and clearing ROS [52,53]. With the excessive ROS-scavenging ability, ShedWise can significantly alleviate ROS production in HUVEC, endowing the vascular cells to display better pro-endothelial functions in later stages.

The morphology of HUVEC adhered on different substrates was further compared after staining of their cytoskeleton and nucleus (Fig. S11). Compared to those on the PPFU surface, the HUVEC had a more extended shape on the PF-HB, PF-RE, and PF-H/R surfaces. Most of the cells were well spreading with a slender and cobblestone morphology, which is consistent with the previous observation [54], indicating that the HBPL grafting is conducive to cell adhesion and spreading. The REDV promoted the HUVEC adhesion and spreading to a larger degree. By contrast, the number of cells adhered on ShedWise was limited without apparent pseudopodia, due to the anti-adhesion performance of the hydrophilic self-sacrificing coating.

To simulate the potential HUVEC adhesion along with the degradation of sacrificing coating, the ShedWise was pre-treated with H_2O_2 solution for varying durations before cell seeding (Fig. 4d and e). There were extremely low HUVEC (0.12 ± 0.05 %) adhered on the surface without H_2O_2 treatment. Along with the prolongation of degradation time, the area of fluorescence gradually increased and reached 5.09 ± 1.26 % (corresponding to the degradation rate of nearly 80 % under dynamic simulated conditions *in vitro*) at 120 h.

These results are aligned with the anticipated cellular responses upon the degradation of the coating. In a normal environment, the coating enriched with HBPAK initially exhibits shedding behavior, effectively deterring protein and cell adhesion, and thereby resisting cell recruitment during the early stages. As the hydrogel coating gradually degrades under oxidative conditions, the intermediate HBPL-REDV layer is exposed, which then serves as a recruiter for endothelial cells. This process facilitates a transformation from an "anti-adhesion" to a "colonization-promoting" effect within the ShedWise system.

The over-proliferation of SMC leads to intimal hyperplasia. The presence of proliferative tissue can impede the attachment and expansion of new endothelial cells, thereby obstructing the process of endothelialization. To simulate the injured site where multiple cell types co-exist and to assess the regulatory effect of ShedWise on competitive cell adhesion, a co-culture model of HUVEC (green) and SMC (red) was carried out (Fig. 4f and g). Compared to the control group, SMC proliferated as a priority over HUVEC on PPFU. Under the H_2O_2 treatment, cells release inflammatory mediators such as interleukin (i.e., IL-6, IL-8) and tumor necrosis factor (i.e., TNF-α), which contribute to the promotion of SMC growth [55]. After modification, both the PF-RE and ShedWise groups exhibited selective proliferation effects on HUVEC. Furthermore, the ShedWise group enhanced the adhesion of HUVEC than SMC significantly. Therefore, the ShedWise effectively integrates cell protection with selective affinity for endothelial cells.

2.5. Assessment of ShedWise in vivo

The assessment of the coating *in vivo* was conducted by employing an abdominal aorta wire injury model in rats (Fig. 5a and b, and Fig. S12a). The vascular injuries were subjected to treatment with PPFU, PF-HB, PF-RE, PF-H/R, and ShedWise, respectively. The final evaluation time was 14 d post-surgery, because this timeframe is acknowledged as a complete cycle of re-endothelialization in blood vessels [56,57].

To allow the ease of observation and quantification, ShedWise prepared from cyanine5.5 NHS ester (Cy5.5)-labeled HBPAK was implanted in the rat's aorta, and was taken out for assessment *ex vivo* along with time prolongation (Fig. 5c). A monotonous reduction of fluorescent intensity was observed, suggesting the continuous degradation of the self-sacrificing coating. On day 7, the fluorescence intensity disappeared completely, indicating a complete "sacrifice" of the top hydrogel coating (Fig. 5d). This change is in good agreement with the dynamic simulated degradation *in vitro*, conveying the possibility of restoring homeostasis at the initial stage, and subsequent exposure of the HBPL-REDV layer for endothelial recovery.

During vascular injury, SMC de-differentiates from a quiescent state to a synthetic state, thereby enhancing their proliferation and migration capabilities, leading to intimal hyperplasia, which is detrimental to the blood flow patency and long-term vascular stability [58,59]. The intima hyperplasia was assessed by Masson's trichrome staining of cross-sections (Fig. 5e), where the unbounded region growing from the intima toward the vascular lumen was identified as neointimal proliferation. Evident neointimal formation was observed in the Model group, which was largely restricted by all the materials-implanting groups, suggesting that these materials function similarly to those covered stents in clinical applications by providing support to prevent elastic recoil and neointimal hyperplasia [60,61]. In particular, the tunica media of PF-HB and ShedWise was only thickened slightly (Fig. S12b), which is potentially associated with the proliferation of cells and rebuilding of the matrix in the media region, leading to the repair of the damaged vascular structure and enhancement of its stability [62]. Quantitative analysis of the intima/media (I/M) ratio (Fig. 5f and Figs. S13a and b) reveals that the ShedWise possessed the smallest I/M ratio (0.10 ± 0.05) closest to the normal. Compared to the normal group's lumen area that is 100 %, the ShedWise group had a value of 79.7 % lumen area. A nearly circular tissue was observed at the center of the lumen in the PPFU group (Fig. 5e), which is interpreted as the intraluminal thrombus formation, resulting in a lower lumen patency rate. This finding is consistent with the *in vitro* hemocompatibility results. In conclusion, the ShedWise effectively prevents excessive intimal hyperplasia and thrombus formation *in vivo*, thereby maintaining a better level of lumen patency close to that of the normal group (Fig. 5g).

Following vascular injuries, monocytes migrate toward the damaged sites and differentiate into macrophages, which play a crucial role in regulating vascular tissue regeneration through the secretion of cytokines and growth factors. The inflammatory (M1) and anti-inflammatory (M2) phenotypes of macrophages were stained with CD86 and CD163 to assess their infiltration (Figure S14 and Figure S15a,

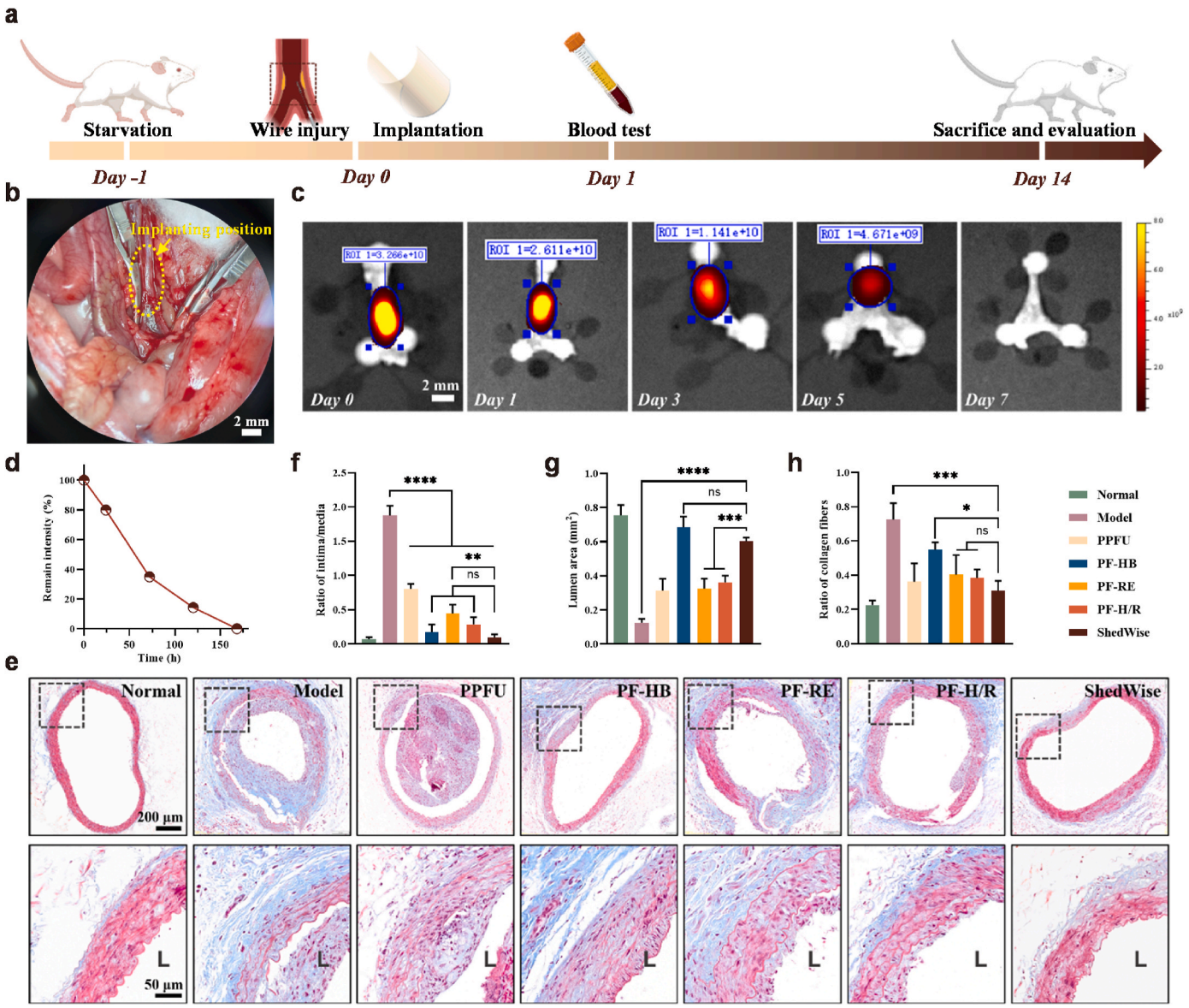

Fig. 5. Degradation behavior of the self-sacrificing coating and its effect on intimal hyperplasia *in vivo*. (a) Schematic illustration of wire injuries in the rat abdominal aorta. The membranes of different groups were implanted immediately after injuries. (b) Real-time microscopic image of the aorta in surgery. (c) Fluorescence intensity loss of self-sacrificing coating during 7 d degradation after implantation. The blood vessels were collected at specific time intervals after implantation, and were imaged *ex vivo*. (d) Quantification of fluorescence intensity over time. (e) Representative Masson's trichrome staining of treated aortas at 14 d after surgery ("L" in each image represents lumen). Quantification of (f) ratio of intima/media, (g) lumen area, and (h) ratio of collagen fibers (n = 3). *p < 0.05, **p < 0.01, ***p < 0.001 and ****p < 0.0001; ns = no significant difference.

b), respectively. Compared to the larger number of $CD86^+$ cells observed in the Model, PPFU and PF-HB groups (3.8, 2.6, and 4.6 cells per field, respectively), fewer ones were found in the PF-RE, PF-H/R, and ShedWise groups (0.6, 0.8 and 0.6 cells per field, respectively). In the subluminal areas of the treated aortas, the reduced M1 macrophages and elevated M2 macrophages indicate a decreased level of inflammation. This reduction trend is positively associated with the existence of REDV peptide and self-sacrificing coating in ShedWise, which is consistent with their stronger anti-oxidation ability *in vitro*.

The excessive inflammatory response at the injured site of the aorta will also cause an increase in inflammation levels throughout the body. Elisa test was conducted to evaluate the levels of inflammatory factors of IL-6, TNF-α, and IL-10 in rat serum after 1 d of surgery (Fig. 6a–c). The ShedWise demonstrated the most pronounced effect on the reduction of IL-6 and TNF-α, highlighting its strong ability to mitigate acute inflammation at the injury site. Meanwhile, both the PF-H/R and ShedWise upregulated the IL-10 level compared to the Model group, suggesting that they help regulate the immune response, reduce inflammation, and support the subsequent healing and recovery of the tissue as shown below.

The degree of fibrosis in the adventitia and surrounding tissues has an intrinsic relationship with the inflammatory responses after vascular injuries. Here, the ratio of fibrosis degree was analyzed. Fig. 5e–h shows that the PF-RE, PF-H/R, and ShedWise groups reduced the fibrosis significantly compared to the Model group, which is consistent with the macrophage infiltration degree. Therefore, surface modification with REDV peptides and the self-sacrificing coating reduces inflammation while simultaneously promoting vascular healing.

The final phase of the intima recovery involves the formation of a fully developed endoderm, resembling the original natural endothelial structure. Immunofluorescent staining at 14 d post-surgery (Fig. 6d) reveals that the coverage of endothelium in the Model group with a

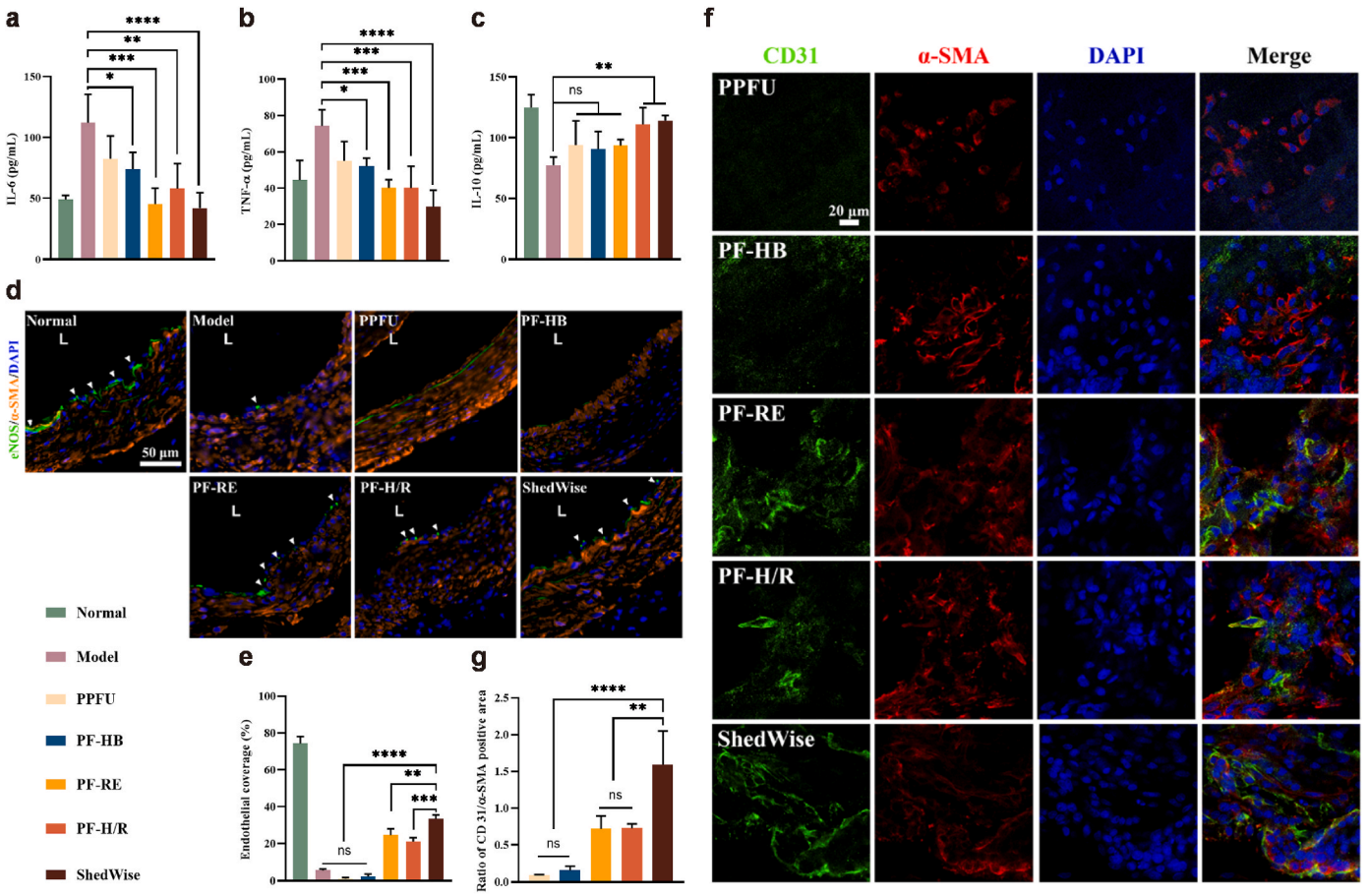

Fig. 6. Effects of sample treatment on inflammatory modulation and endothelial recovery. Quantitative results of (a) IL-6, (b) TNF-α, and (c) IL-10 level in rat serum 1 d post-surgery by Elisa tests (n = 4). (d) Representative eNOS (green) and α-SMA (orange) double staining of aortas from different groups at 14 d after surgery. (e) Quantification of endothelial coverage from images in (d) (n = 3). (f) Representative confocal images showing CD31 (green) and α-SMA (red) expression on different samples at 14 d after surgery. (g) Ratio of CD31/α-SMA positive area from images in (f) (n = 3). *p < 0.05, **p < 0.01, ***p < 0.001 and ****p < 0.0001; ns = no significant difference.

value of 5.6 ± 0.9 % (Fig. 6e) was notably low. By contrast, the endothelium coverage reached the highest value of 33.5 ± 2.5 % in the ShedWise group, demonstrating its capacity to enhance endothelium regeneration. The aortas treated with PF-RE and PF-H/R exhibited endothelium coverage of 24.7 ± 2.5 % and 21.1 ± 2.2 %, respectively. Meanwhile, a contrasting trend in the α-SMA positive areas was observed (Fig. S16a). These results suggest that the PF-H/R encourages endothelium regeneration, particularly when combined with the self-sacrificing coating. The increased degree of endothelialization can inhibit the migration of underlying SMC to some extent, thereby facilitating the subsequent formation of the endodermis.

On the other hand, the pro-endothelial functions on the materials' surface facing the blood flow at 14 d were assessed by immunofluorescence staining of CD31 (Fig. 6f). The inner surface of ShedWise exhibited a relatively continuous CD31-positive area (green), closely resembling the structure of normal vascular endothelium compared to other groups. The coverage of endothelial cells (9.1 ± 0.9 %) was more complete than that of PF-H/R (5.4 ± 0.3 %) (Fig. S16b). Additionally, α-SMA was used to label SMC that migrated to the inner surface of the vascular graft. The ShedWise group exhibited the highest CD31/α-SMA positive area ratio (1.6 ± 0.4), which is 2 folds of that of the PF-H/R group (0.7 ± 0.1) (Figure S16c and Fig. 6g). This result highlights the importance of the self-sacrificing layer in suppressing SMC colonization, promoting endothelialization, and effectively mitigating intimal proliferation during vascular repair.

Moreover, a multilayer scanning and 3D reconstruction of the ShedWise group (Fig. S17a) reveals continuous green signals, indicating the formation of tight junctions between the endothelial cells. No significant increase in α-SMA expression was observed, suggesting that our material supports vascular repair rather than inducing an endothelial-to-mesenchymal transition (EndMT). SEM observation of the neointima on the inner surface (Fig. S17b) reveals that after 14 d of implantation, the ShedWise exhibited a regular surface morphology similar to that of natural endothelium, and possessed obvious spindle cell structure on the magnification images. By contrast, the surface structure of PPFU appeared disordered, with blood cells and protein fibers deposited on the surface shown in the higher magnification images.

Lastly, the lung, liver, spleen, kidney, and heart of rats were harvested for H&E staining to explore the possible influence of metabolites (Fig. S18). All the physiological structures and cell morphology of organs were normal, indicating that all the groups had no toxicity and possessed favorable biosafety *in vivo*.

In summary, our ShedWise has shown positive effects on preventing intimal hyperplasia, modulating inflammatory environment, and promoting re-endothelialization. The experimental results *in vivo* and *in vitro* demonstrate the efficacy of our design of ShedWise as listed below: (1) the top hydrogel coating-mediated ROS scavenging for antioxidation and modification of the inflammatory environment; (2) controllable self-degradation properties and optimal blood compatibility of the self-sacrificing coating; (3) HBPL-REDV-mediated specific endothelial cells recruitment. Because of the availability of materials used and the ease of preparation, our strategy can be adapted to a range of surfaces and various implantable cardiovascular devices, including absorbable stents, vascular patches, and heart valves, thereby facilitating treatment and

promoting tissue regeneration. Overall, the Shedvise offers a novel perspective for developing a therapeutic platform addressing vascular injuries and other diseases characterized by temporal dynamics across different stages.

3. Conclusion

The acute inflammatory response induced by interventional surgeries and subsequent challenges in endothelial recovery is crucial for the normal functionality of cardiovascular implants. In this study, we have innovatively developed a "multi-in-one" device of ShedWise, which orchestrated the interaction between implanted devices and target sites in a cascade. The top HBPAK coating effectively reduced ROS level, and meanwhile exhibited controlled self-degradation properties and optimal blood compatibility. Under an oxidative environment, the ShedWise displayed notable protective and antioxidative effects on HUVEC. By regulating the abnormal inflammatory microenvironment, the HBPL-REDV layer specifically stimulated endothelial cell growth. Consequently, every phase from the post-injury to the restoration of the endothelial barrier at the implantation site was mediated consecutively and appropriately. The degradation rate of the ROS-sensitive layer can be easily tailored to balance the anti-inflammatory and pro-regenerative functions at diverse pathological conditions. By this "self-sacrificing to pro-endothelial" cascade strategy, our ShedWise demonstrated its robust efficacy in protecting damaged tissues, promoting re-endothelialization, and reducing final restenosis in a vascular injury model. This strategy provides a viable solution for enhancing the treatment and prognosis of interventional therapies of cardiovascular implants, and demonstrates potential for surface engineering in other intravascular devices.

CRediT authorship contribution statement

Pai Peng: Writing – review & editing, Writing – original draft, Visualization, Validation, Methodology, Investigation, Formal analysis, Data curation, Conceptualization. **Shili Ding:** Writing – original draft, Methodology, Investigation, Formal analysis, Data curation. **Min Liang:** Methodology, Investigation, Data curation. **Weiwei Zheng:** Methodology, Investigation. **Yongyuan Kang:** Methodology, Investigation. **Wenxing Liu:** Supervision, Project administration. **Haifei Shi:** Writing – review & editing, Supervision, Resources, Project administration, Conceptualization. **Changyou Gao:** Writing – review & editing, Supervision, Resources, Project administration, Funding acquisition, Conceptualization.

Ethics approval and consent to participate

All animal experiments in this study were conducted in strict accordance with the guidelines and regulations for the care and use of laboratory animals and were approved by the Lab of Animal Experimental Ethical Inspection of Dr. Can Biotechnology (Zhejiang) Co., Ltd (Application number: DRK2023150284). The experimental protocols were designed to minimize animal suffering and adhere to the principles of the 3Rs (Replacement, Reduction, and Refinement).

Declaration of Competing Interests

The authors declare that they have no known competing financial interests or personal relationships that could have appeared to influence the work reported in this paper.

Acknowledgements

This study is financially supported by the Joint Fund of National Natural Science Foundation of China (U22A20155), the Lingyan Program of Zhejiang Province (2022C01106), the State Key Laboratory of Transvascular Implantation Devices (012024004), the ZJU DPSE-NEWMED Biomedical Polymers and Devices Research & Development Lab, and the 111 Project (B16042).

Appendix A. Supplementary data

Supplementary data to this article can be found online at https://doi.org/10.1016/j.bioactmat.2025.01.037.

References

[1] B. Bay, C. Blaum, C. Kellner, R. Bei der Kellen, F. Ojeda, J. Waibel, N. Arnold, C. A. Behrendt, D.L. Rimmele, G. Thomalla, R. Twerenbold, S. Blankenberg, B. Zyriax, F.J. Brunner, C. Waldeyer, Inflammatory burden, lifestyle and atherosclerotic cardiovascular disease: insights from a population based cohort study, Sci. Rep. 13 (2023) 21761.

[2] D. Zhao, J. Liu, M. Wang, X. Zhang, M. Zhou, Epidemiology of cardiovascular disease in China: current features and implications, Nat. Rev. Cardiol. 16 (2019) 203–212.

[3] S. Rehman, E. Rehman, A. Mumtaz, Z. Jianglin, Cardiovascular disease mortality and potential risk factor in China: a multi-dimensional assessment by a grey relational approach, Int. J. Public Health. 67 (2022) 1604599.

[4] X. Hu, S. Li, P. Peng, B. Wang, W. Liu, X. Dong, X. Yang, M. Karabaliev, Q. Yu, C. Gao, Prosthetic heart valves for transcatheter aortic valve replacement, BMEMat 1 (2023) e12026.

[5] Y. Snyder, S. Jana, Strategies for development of synthetic heart valve tissue engineering scaffolds, Prog. Mater. Sci. 139 (2023) 101173.

[6] Y. Li, Y. Shi, Y. Lu, X. Li, J. Zhou, A.A. Zadpoor, L. Wang, Additive manufacturing of vascular stents, Acta Biomater. 167 (2023) 16–37.

[7] K. Kwon, J.U. Kim, S.M. Won, J. Zhao, R. Avila, H. Wang, K.S. Chun, H. Jang, K. H. Lee, J.-H. Kim, S. Yoo, Y.J. Kang, J. Kim, J. Lim, Y. Park, W. Lu, T. Kim, A. Banks, Y. Huang, J.A. Rogers, A battery-less wireless implant for the continuous monitoring of vascular pressure, flow rate and temperature, Nat. Biomed. Eng. 7 (2023) 1215–1228.

[8] J.S. Greer, M.A. Hussein, R. Vamsee, Y. Arar, S. Krueger, S. Weiss, J. Dillenbeck, G. Greil, S.R. Veeram Reddy, T. Hussain, Improved catheter tracking during cardiovascular magnetic resonance-guided cardiac catheterization using overlay visualization, J. Cardiovasc. Magn. Reson. 24 (2022) 32.

[9] F. Otsuka, A.V. Finn, S.K. Yazdani, M. Nakano, F.D. Kolodgie, R. Virmani, The importance of the endothelium in atherothrombosis and coronary stenting, Nat. Rev. Cardiol. 9 (2012) 439–453.

[10] T. Gori, Endothelial Function: a short guide for the interventional cardiologist, Int. J. Mol. Sci. 19 (2018) 3838.

[11] M. Kheifets, O. Rahat, T. Bental, A. Levi, H. Vaknin-Assa, G. Greenberg, P. Codner, G. Witberg, R. Kornowski, L. Perl, Outcomes of drug eluting balloons for in-stent restenosis: large cohort analysis and single center clinical experience, Can. J. Cardiol. 40 (2024) 1250–1257.

[12] A.H. Ates, A. Kivrak, S. Zekeriyeyev, C. Menemencioglu, C. Coteli, N. Ozer, M. L. Sahiner, E.B. Kaya, Unlocking promising therapies: drug-eluting stents in medically refractory angina patients with myocardial bridging, Am. J. Cardiol. 208 (2023) 72–74.

[13] J. Yin, Y. Li, Y. Chen, C. Wang, X. Song, Biodegradable polymer everolimus-eluting stents versus contemporary drug-eluting stents: a systematic review and meta-analysis, Sci. Rep. 13 (2023) 1715.

[14] R. Waksman, K.R. Chitturi, Myths and truths in the management of drug-eluting stent in-stent restenosis, JACC Cardiovasc. Interv. 17 (2024) 14–16.

[15] B. Cortese, G. Testa, F. Rivero, A. Erriquez, F. Alfonso, Long-term outcome of drug-coated balloon vs drug-eluting stent for small coronary vessels: PICCOLETO-II 3-year follow-up, JACC Cardiovasc. Interv. 16 (2023) 1054–1061.

[16] E. Ho, K. Denby, S. Cherian, J. Ciezki, M. Kolar, D. Wilkinson, J. Wagener, L. Young, A. Essa, S. Ellis, Intracoronary brachytherapy for drug-eluting stent restenosis: outcomes and clinical correlates, J. Soc. Cardiovasc. Angiogr. Interv. 2 (2023) 100550.

[17] U.M. Balaguru, L. Sundaresan, J. Manivannan, R. Majunathan, K. Mani, A. Swaminathan, S. Venkatesan, D. Kasiviswanathan, S. Chatterjee, Disturbed flow mediated modulation of shear forces on endothelial plane: a proposed model for studying endothelium around atherosclerotic plaques, Sci. Rep. 6 (2016) 27304.

[18] D. Wang, T. Brady, L. Santhanam, S. Gerecht, The extracellular matrix mechanics in the vasculature, Nat. Cardiovasc. Res. 2 (2023) 718–732.

[19] V. Mehta, K.L. Pang, C.S. Givens, Z. Chen, J. Huang, D.T. Sweet, H. Jo, J.S. Reader, E. Tzima, Mechanical forces regulate endothelial-to-mesenchymal transition and atherosclerosis via an Alk5-Shc mechanotransduction pathway, Sci. Adv. 7 (2021) eabg5060.

[20] S. Stojkovic, C. Kaun, J. Basilio, S. Rauscher, L. Hell, K.A. Krychtiuk, C. Bonstingl, R. de Martin, M. Gröger, C. Ay, W. Holnthoner, W. Eppel, C. Neumayer, I. Huk, K. Huber, S. Demyanets, J. Wojta, Tissue factor is induced by interleukin-33 in human endothelial cells: a new link between coagulation and inflammation, Sci. Rep. 6 (2016) 25171.

[21] P. Kong, Z.Y. Cui, X.F. Huang, D.D. Zhang, R.J. Guo, M. Han, Inflammation and atherosclerosis: signaling pathways and therapeutic intervention, Signal Transduct. Targeted Ther. 7 (2022) 131.

[22] P. Libby, Inflammation and the pathogenesis of atherosclerosis, Vasc. Pharmacol. 154 (2024) 107255.

[23] S. Guerra-Ojeda, P. Marchio, C. Rueda, A. Suarez, H. Garcia, V.M. Victor, M. Juez, I. Martin-Gonzalez, J.M. Vila, M.D. Mauricio, Cerium dioxide nanoparticles modulate antioxidant defences and change vascular response in the human saphenous vein, Free Radic. Biol. Med. 193 (2022) 694–701.
[24] C.L. Wee, S.S. Mokhtar, K.K. Banga Singh, A.H.G. Rasool, Vitamin D deficiency attenuates endothelial function by reducing antioxidant activity and vascular eNOS expression in the rat microcirculation, Microvasc. Res. 138 (2021) 104227.
[25] J. Zhao, J. Fu, F. Jia, J. Li, B. Yu, Y. Huang, K. Ren, J. Ji, G. Fu, Precise regulation of inflammation and oxidative stress by ROS-responsive prodrug coated balloon for preventing vascular restenosis, Adv. Funct. Mater. (2023) 2213993.
[26] R. Mata, Y. Yao, W. Cao, J. Ding, T. Zhou, Z. Zhai, C. Gao, The dynamic inflammatory tissue microenvironment: signality and disease therapy by biomaterials, Research 2021 (2021) 4189516.
[27] Y. Yao, Reactive oxygen species (ROS)-responsive biomaterials mediate tissue microenvironments and tissue regeneration, J. Mater. Chem. B 7 (2019) 5019–5037.
[28] H. Ye, Y. Zhou, X. Liu, Y. Chen, S. Duan, R. Zhu, Y. Liu, L. Yin, Recent advances on reactive oxygen species-responsive delivery and diagnosis system, Biomacromolecules 20 (2019) 2441–2463.
[29] B. Hu, C. Ye, C. Gao, Synthesis and characterization of biodegradable polyurethanes with unsaturated carbon bonds based on poly(propylene fumarate), J. Appl. Polym. Sci. 132 (2015) 42065.
[30] H.L. Pu, W.L. Chiang, B. Maiti, Z.X. Liao, Y.C. Ho, M.S. Shim, E.Y. Chuang, Y. Xia, H.W. Sung, Nanoparticles with dual responses to oxidative stress and reduced pH for drug release and anti-inflammatory applications, ACS Nano 8 (2014) 1213–1221.
[31] M.S. Shim, Y. Xia, A reactive oxygen species (ROS)-responsive polymer for safe, efficient, and targeted gene delivery in cancer cells, Angew. Chem. Int. Ed. 52 (2013) 6926–6929.
[32] D.S. Wilson, G. Dalmasso, L. Wang, S.V. Sitaraman, D. Merlin, N. Murthy, Orally delivered thioketal nanoparticles loaded with TNF-α–siRNA target inflammation and inhibit gene expression in the intestines, Nat. Mater. 9 (2010) 923–928.
[33] D.W. Essex, L. Wang, Recent advances in vascular thiol isomerases and redox systems in platelet function and thrombosis, J. Thromb. Haemostasis 22 (2024) 1806–1818.
[34] Y. Yu, H. Yuk, G.A. Parada, Y. Wu, X. Liu, C.S. Nabzdyk, K. Youcef-Toumi, J. Zang, X. Zhao, Multifunctional "hydrogel skins" on diverse polymers with arbitrary shapes, Adv. Mater. 31 (2019) 1807101.
[35] G. Parada, Y. Yu, W. Riley, S. Lojovich, D. Tshikudi, Q. Ling, Y. Zhang, J. Wang, L. Ling, Y. Yang, S. Nadkarni, C. Nabzdyk, X. Zhao, Ultrathin and robust hydrogel coatings on cardiovascular medical devices to mitigate thromboembolic and infectious complications, Adv. Healthcare Mater. 9 (2020) 2001116.
[36] Y. Yu, J. Wang, X. Wang, Y. Huang, R. Li, Y. Wang, K. Ren, J. Ji, A tough, slippery, and anticoagulant double-network hydrogel coating, ACS Appl. Polym. Mater. 4 (2022) 5941–5951.
[37] J. Liu, S. Qu, Z. Suo, W. Yang, Functional hydrogel coatings, Natl. Sci. Rev. 8 (2021) nwaa254.
[38] S. Torii, H. Jinnouchi, A. Sakamoto, M. Kutyna, A. Cornelissen, S. Kuntz, L. Guo, H. Mori, E. Harari, K.H. Paek, R. Fernandez, D. Chahal, M.E. Romero, F. D. Kolodgie, A. Gupta, R. Virmani, A.V. Finn, Drug-eluting coronary stents: insights from preclinical and pathology studies, Nat. Rev. Cardiol. 17 (2020) 37–51.
[39] H. Yuk, T. Zhang, S. Lin, G.A. Parada, X. Zhao, Tough bonding of hydrogels to diverse non-porous surfaces, Nat. Mater. 15 (2016) 190–196.
[40] C. Pan, X. Liu, Q. Hong, J. Chen, Y. Cheng, Q. Zhang, L. Meng, J. Dai, Z. Yang, L. Wang, Recent advances in surface endothelialization of the magnesium alloy stent materials, J. Magnesium Alloys 11 (2023) 48–77.
[41] L. Wang, R. Xu, L. Meng, Q. Zhang, Z. Qian, J. Chen, C. Pan, A fucoidan-loaded hydrogel coating for enhancing corrosion resistance, hemocompatibility and endothelial cell growth of magnesium alloy for cardiovascular stents, Biomater. Adv. 163 (2024) 213960.
[42] C. Pan, N. Yang, J. Chen, Q. Hong, L. Zhu, B. Zhang, Constructing NO/CO gases-releasing bioactive coating to synergistically enhance corrosion resistance and biocompatibility of magnesium alloy for cardiovascular stents, Colloids Surf. A Physicochem. Eng. Asp. 704 (2025) 135521.
[43] I. Fishbein, R.F. Adamo, M. Chorny, R.J. Levy, Abstract 20621: longitudinal detection of ROS production in balloon-injured arteries by bioluminescence imaging, Circulation 122 (2010). A20621–A20621.
[44] J. Ding, Y. Yao, J. Li, Y. Duan, J.R. Nakkala, X. Feng, W. Cao, Y. Wang, L. Hong, L. Shen, Z. Mao, Y. Zhu, C. Gao, A reactive oxygen species scavenging and O_2 generating injectable hydrogel for myocardial infarction treatment in vivo, Small 16 (2020) 2005038.
[45] M.P. Murphy, H. Bayir, V. Belousov, C.J. Chang, K.J.A. Davies, M.J. Davies, T. P. Dick, T. Finkel, H.J. Forman, Y. Janssen-Heininger, D. Gems, V.E. Kagan, B. Kalyanaraman, N.G. Larsson, G.L. Milne, T. Nyström, H.E. Poulsen, R. Radi, H. Van Remmen, P.T. Schumacker, P.J. Thornalley, S. Toyokuni, C.C. Winterbourn, H. Yin, B. Halliwell, Guidelines for measuring reactive oxygen species and oxidative damage in cells and in vivo, Nat. Metab. 4 (2022) 651–662.
[46] G. Apte, J. Börke, H. Rothe, K. Liefeith, T.H. Nguyen, Modulation of platelet-surface activation: current state and future perspectives, ACS Appl. Bio Mater. 3 (2020) 5574–5589.
[47] B. Yi, L. Yu, H. Tang, W. Wang, W. Liu, Y. Zhang, Lysine-doped polydopamine coating enhances antithrombogenicity and endothelialization of an electrospun aligned fibrous vascular graft, Appl. Mater. Today 25 (2021) 101198.
[48] P. Kaur, D. Sethi, M.D. Hade, J. Kaur, K.L. Dikshit, C-terminal lysine residues enhance plasminogen activation by inducing conformational flexibility and stabilization of activator complex of staphylokinase with plasmin, Arch. Biochem. Biophys. 743 (2023) 109671.
[49] J. Liu, X. Han, T. Zhang, K. Tian, Z. Li, F. Luo, Reactive oxygen species (ROS) scavenging biomaterials for anti-inflammatory diseases: from mechanism to therapy, J. Hematol. Oncol.J Hematol Oncol. 16 (2023) 116.
[50] C.A. Juan, J.M. Pérez de la Lastra, F.J. Plou, E. Pérez-Lebeña, The chemistry of reactive oxygen species (ROS) revisited: outlining their role in biological macromolecules (DNA, lipids and proteins) and induced pathologies, Int. J. Mol. Sci. 22 (2021) 4642.
[51] S. Xu, I. Ilyas, P.J. Little, H. Li, D. Kamato, X. Zheng, S. Luo, Z. Li, P. Liu, J. Han, I. C. Harding, E.E. Ebong, S.J. Cameron, A.G. Stewart, J. Weng, Endothelial dysfunction in atherosclerotic cardiovascular diseases and beyond: from mechanism to pharmacotherapies, Pharmacol. Rev. 73 (2021) 924–967.
[52] A. Mahara, K. Kitagawa, A. Otaka, T. Nakaoki, K. Ishihara, T. Yamaoka, Impact of REDV peptide density and its linker structure on the capture, movement, and adhesion of flowing endothelial progenitor cells in microfluidic devices, Mater. Sci. Eng. C. 129 (2021) 112381.
[53] B. Zhang, Y. Qin, Y. Wang, A nitric oxide-eluting and REDV peptide-conjugated coating promotes vascular healing, Biomaterials 284 (2022) 121478.
[54] Z. Yang, Y. Xi, J. Bai, Z. Jiang, S. Wang, H. Zhang, W. Dai, C. Chen, Z. Gou, G. Yang, C. Gao, Covalent grafting of hyperbranched poly-L-lysine on Ti-based implants achieves dual functions of antibacteria and promoted osteointegration in vivo, Biomaterials 269 (2021) 120534.
[55] M. Hutton, M. Frazer, A. Lin, S. Patel, A. Misra, New targets in atherosclerosis: vascular smooth muscle cell plasticity and macrophage polarity, Clin. Therapeut. 45 (2023) 1047–1054.
[56] G. Santulli, A. Wronska, K. Uryu, T.G. Diacovo, M. Gao, S.O. Marx, J. Kitajewski, J. M. Chilton, K.M. Akat, T. Tuschl, A.R. Marks, H. Totary-Jain, A selective microRNA-based strategy inhibits restenosis while preserving endothelial function, J. Clin. Invest. 124 (2014) 4102–4114.
[57] R. Cartier, P. Pearson, P. Lin, H. Schaff, Time course and extent of recovery of endothelium-dependent contractions and relaxations after direct arterial injury, J. Thorac. Cardiovasc. Surg. 102 (1991) 371–377.
[58] G.K. Owens, M.S. Kumar, B.R. Wamhoff, Molecular regulation of vascular smooth muscle cell differentiation in development and disease, Physiol. Rev. 84 (2004) 767–801.
[59] G.L. Basatemur, H.F. Jørgensen, M.C.H. Clarke, M.R. Bennett, Z. Mallat, Vascular smooth muscle cells in atherosclerosis, Nat. Rev. Cardiol. 16 (2019) 727–744.
[60] K. Toutouzas, C. Stefanadis, E. Tsiamis, L. Khaldi, K. Tentolouris, A. Doufas, A. Michaelides, P. Toutouzas, Autologous vascular graft-covered stents: effect on endothelialization, intimal hyperplasia and vascular injury in porcine coronary arteries, J. Am. Coll. Cardiol. 35 (2000), 79A-79A.
[61] M.L. Marin, F.J. Veith, J. Cynamon, R.E. Parsons, R.T. Lyon, W.D. Suggs, C. W. Bakal, S. Waahl, L.A. Sanchez, J.C. Yuan, T. Ohki, Effect of polytetrafluoroethylene covering of Palmaz stents on the development of intimal hyperplasia in human iliac arteries, J. Vasc. Intervent. Radiol. 7 (1996) 651–656.
[62] J. Tang, H. Wang, X. Huang, F. Li, H. Zhu, Y. Li, L. He, H. Zhang, W. Pu, K. Liu, H. Zhao, J.F. Bentzon, Y. Yu, Y. Ji, Y. Nie, X. Tian, L. Zhang, D. Gao, B. Zhou, Arterial sca1+ vascular stem cells generate de novo smooth muscle for artery repair and regeneration, Cell Stem Cell 26 (2020) 81–96.e4.